Numerical Modeling of the Test Pit for Falling Weight Deflectometer Calibration
Task 1 and 2 Report – Draft

by

Mohammadhossein Sadeghiamirshahidi, Ph.D., A.M. ASCE.
Assistant Professor, Geological Engineering
Marvin Speece, Ph.D.
Professor, Geophysics

Affiliation
Montana Technological University

Submitted to:

Montana Department of Transportation
2701 Prospect Avenue
P.O. Box 201001
Helena, MT 59620-1001

02/08/2021

1. TABLE OF CONTENTS

2. LIST OF TABLES

3. LIST OF FIGURES

4. PROBLEM STATEMENT

Evaluation of pavement sections is commonly conducted using the deflection data from Falling Weight Deflectometer (FWD) tests. The reliability of these evaluations is highly dependent on the accuracy of the measured deflections. Therefore, to ensure the desired accuracy of measured deflections, FWDs undergo annual calibration and monthly relative calibrations. These calibrations are conducted according to AASHTO R32-11 [1]. The calibration tests are conducted on an indoor test pit made of a concrete slab underlaid by a base and a soft subgrade.

The calibration facility operated by the Montana Department of Transportation (MDT) has used a 12 ft wide, 15 ft long, and 5 in thick concrete slab overlying a 6-in thick sandy base and a 4-ft thick clay subgrade (R32 design, Figure 1). The measured deflections during calibration tests conducted by MDT on this test pit met the deflection requirements laid out by AASHTO R32-11 for a few years, after which the test area needed to be replaced. Because rebuilding the test area is both costly and time-consuming, the MDT was interested in a new design that could operate over longer periods. MDT designed an alternative to the R32 design, using geofoam instead of the clay layer as the soft subgrade (Figure 2).

Figure 1. Schematic as-built cross-section of the MDT's original testing area (not to scale).

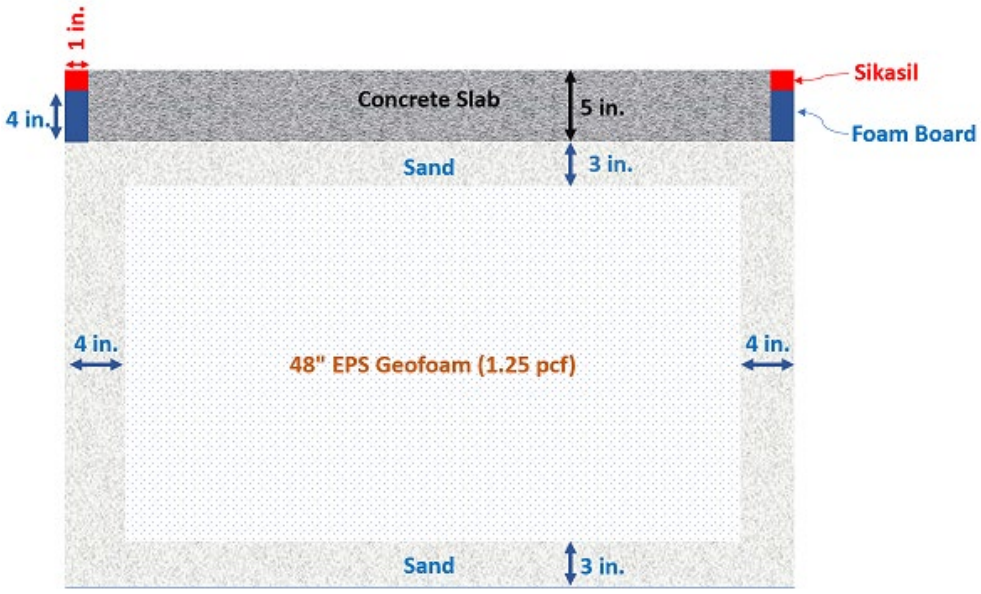

Figure 2. Schematic as-built cross-section of the MDT's preliminary alternative testing area (not to scale).

The alternative calibration test pit (geofoam test pit) was designed based on static analyses. The designed test area was constructed, and several FWD calibration tests were conducted. The new setup did not meet the AASHTO R32-11 deflection requirements. Also, some deflections (noise) upon initiation of the falling weight (before the weight actually hits the plate) were detected by the sensors during the calibration tests conducted on the geofoam test pit. The purpose of this study is to use dynamic response analyses to investigate the possibility of using geofoam instead of the clay layer in the test pit. If the results of the investigation reveal that geofoam can in fact be used, the next goal of this study will be to modify the preliminary alternative design and provide recommendations to improve the performance of the test area to where it meets the AASHTO R32-11 deflection requirements.

5. BACKGROUND AND LITERATURE REVIEW

Management of pavement systems, at the project or network level, relies on the structural evaluation of pavements which entails approximating the remaining pavement life, estimating load-supporting capacity, and calculating the required thickness of structural overlays. Deflection data from Falling Weight Deflectometers (FWDs) are the basis of such evaluations [2]. For example, one of the key inputs in deterministic physical models used in pavement structural analyses is the moduli of elasticity of the pavement layers [3]. The pavement deflection measured from FWD tests is used to back-calculate the layers' moduli [4–12]. The reliability of the back-calculated moduli, and any analyses conducted based on those moduli, directly depends on the accuracy of the measured deflections. Annual calibration and monthly relative calibrations of the FWDs are therefore necessary to ensure the desired accuracy of the measured deflections. These calibrations are conducted according to AASHTO R32-11 [1] to establish calibration factors for correcting FWD measurements.

AASHTO R32-11 requires the calibration facility to be an indoor space with a constant temperature between 50 and 100°F, heated, but not necessarily air-conditioned. The calibration tests are conducted on a concrete slab with a smooth and crack-free surface. The concrete slab does not have to be isolated from the surrounding floor provided that the deflection characteristics and other requirements for the facility are met. The suggested dimensions for the concrete slab by AASHTO R32-11 are 12 ft by 15 ft (with an 8 ft wide clear zone around the perimeter).

The required deflections in the concrete slab, i.e., 0.012 in or more due to a 16,000-lb load, is generally achieved by using a 5 in thick Portland cement concrete slab underlaid by 8 in of open-graded crushed aggregate base and relatively weak subgrade (subgrade modulus < 12,000 psi when the bedrock is deeper than 25 ft., and subgrade modulus < 7500 psi when the bedrock is between 10 to 25 ft deep, and areas with bedrock located shallower than 10 ft are not recommended).

The calibration facility operated by MDT has used a test pit setup shown in Figure 1. Although the AASHTO's deflection requirements were met using this setup, the short lifetime of the test pit inspired a new more durable test pit design. In their first attempt at designing such a setup, MDT designed an alternative to the R32 design based on static analysis, where they used geofoam instead of the clay subgrade (Figure 2). When tested, the new geofoam test area did not meet the AASHTO R32-11 deflection requirements. Static analyses usually neglect the slab mass and subgrade's damping, despite their importance in the dynamic response of structural elements [13]. Three-dimensional dynamic models, on the other hand, are able to incorporate these crucial factors. For example, one such model has been developed by Kuo et al. [14] and was used to calibrate the back-calculation of pavement layers' stiffnesses. Their model confirmed that subgrade damping and self-weight of the slab which are ignored in static analyses have in fact a significant effect on the results. According to their findings, boundary conditions are another significant factor in modeling FWD deflections. In other research, Foinquinos et al., [15] studied the response of pavements under deflection basin tests (e.g., FWD) and wave propagation tests (e.g., Spectral Analysis of Surface Waves test). Their results confirmed that the magnitude and shape of the deflection basins developed by the FWD tests are affected by the dynamic response of the pavement system and are significantly different from the basins developed by static conditions.

Mallela and George [16] developed a three-dimensional finite element model to study the behavior of pavements under dynamic loading. They first conducted several model runs to evaluate the effects of mesh size and boundary conditions on the results of such models. They concluded that a boundary located at a depth greater than 12.2-m (40-ft) deep does not significantly affect the deflections estimated at the surface. Furthermore, lateral boundaries beyond 9.1 m (30 ft) from the loading area showed negligible effects on the simulation results. It is worth mentioning that they treated the pavement-shoulder interface as a discontinuity, i.e., the shoulder did not provide any structural support to the pavement [16]. They used elastic analysis for all the layers in their models based on the fact that the practical loads applied on the pavements are not likely to exceed the elastic limits of layers. They also found that a fine mesh (element size of 75 mm) around the loaded area with a larger element size farther from the loaded area helps create a nonreflective (quiet) boundary.

Shoukry et al., [17] used finite element models to investigate the effects of doweled or undoweled joints and the spacing between the transverse joints of concrete slabs on the behavior of rigid pavement layers during FWD tests. They compared the deflection basin created in their model with the actual basin measured in experiments which showed the ability of finite element models to simulate the FWD tests. Their results also confirmed that neglecting the dynamic loading condition could lead to unreliable deflection estimates and backcalculation procedures. As in Mallela and George [16], linear elastic behavior was assumed for all layers in this study [17].

William [18] used dynamic finite element models to simulate flexible, rigid, and composite pavement models. They used quiet boundaries at the bottom of all three models. They concluded that a refined mesh is necessary for layers that experience higher stresses (concrete slabs) while a coarser mesh can be used for the base and subgrade. They also added a steel loading plate to their model to increase the accuracy of the loading condition.

Park and Chang [19] applied a two-dimensional plane strain finite element model to investigate the behavior of a flexible pavement structure with EPS geofoam subgrade. Their model consisted of asphalt pavement with a base of crushed rock, subbase of open-aggregate and sand, concrete capping slab, and geofoam subgrade. Their numerical results along with some experimental tests indicated that EPS geofoam can be used as a subgrade in flexible pavements. The deformations predicted by their finite element model were in good agreement with those predicted by AASHTO's flexible pavement design method.

In summary, the published research confirms that dynamic models should be used instead of static models to simulate the behavior of FWD tests. They mostly agree that linear elastic behavior can be assumed for all material in the dynamic model. Mesh size and boundary condition were also shown to be key parameters affecting the results of the models.

6. DATA COLLECTION

In FWD field tests as well as the indoor calibration tests, pavement (concrete slab in calibration tests) deflections caused by the impact from a falling mass are recorded with geophones at different points. The first step in the three-dimensional dynamic modeling of these tests is to determine the falling weight impact loads applied to the concrete. Various magnitudes of impact loads can be induced by FWDs with loading durations of about 20 to 40 milliseconds and a peak at about 10 to 25 milliseconds [20–24]. A typical curve illustrating the impact load-time relations (impact load time history) is shown in Figure 3. The curve was developed based on the data reported by previous researchers [14,16–18]. Because various impact loads can be generated depending on the weight and height of the drop, the normalized stress (stress at any point in time divided by maximum stress) is shown on the y-axis of the plot.

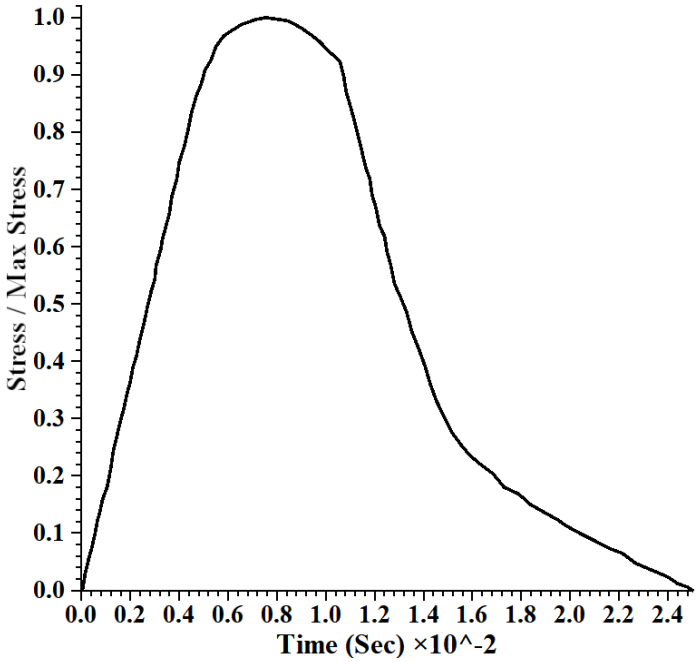

Figure 3. Typical impact load-time relations caused by the weight drop in FWD calibration tests.

The impact load time histories collected during three calibration tests conducted by MDT in December 2019 are shown in Figure 4. These tests were conducted on the geofoam test pit. The general trend recorded in these calibration tests follows that of published data. The corresponding displacements recorded during the aforementioned calibration tests conducted by MDT are also shown in Figure 5.

Unfortunately, the impact load time history data and corresponding displacements recorded during the calibration tests conducted on the clay test pit in 2016 are not available. Some displacement history data from calibration tests conducted on the clay test pit in January 2018 is available but unfortunately, the corresponding impact load time history data is not available. We have discussed this issue with MDT staff, D.J. Berg, P.E. (Pavement Analysis Engineer), and John Amestoy (Non-Destructive Testing Supervisor) in our meeting on Friday 01/29/2021. In a second meeting on Friday 02/05/2021with D.J. Berg, John Amestoy, and Dr. David Orr (Cornell University), it was determined that the impact load-time history data for the clay test pit was not

recorded. However, the data containing the maximum load and maximum displacement caused by those loads exist for calibration tests conducted in January 2018. Some of these data is shown in Table 1. Since the impact load time history is very consistent for FWD calibration tests, we decided in the second meeting, that we can use the existing maximum load and maximum displacement data for the first step of our modeling. The typical impact load-time relation with the collected maximum loads will be assumed for the tests in the model and the maximum displacements predicted by the model will be compared to the collected data in the tests.

Table 1. Some of the maximum load-Maximum Deflection data collected in January 2018 by MDT

Force (kips)	Deflection (mils)
9.01	14.13125
9.01	14.13125
11.94	18.98625
11.98	19.0525
15.1	24.0775
15.14	24.075

Also, the exact location of the weight drop for each one of these tests is not known. This information is required for the modeling. Mr. Amestoy has provided us with an approximate location (within a couple of inches) of the weight drop for the tests conducted on the clay pit in January. It was suggested by the MDT staff to conduct a new set of calibration tests on the geofoam test pit so that the exact location of the weight drop and any other missing data can be collected and be used in the models.

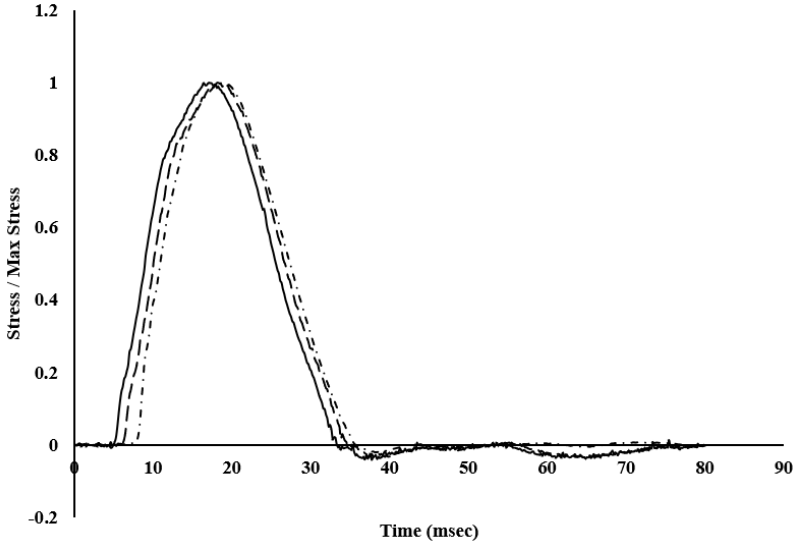

Figure 4. Impact load-time curves of three calibration tests conducted by MDT in December 2019.

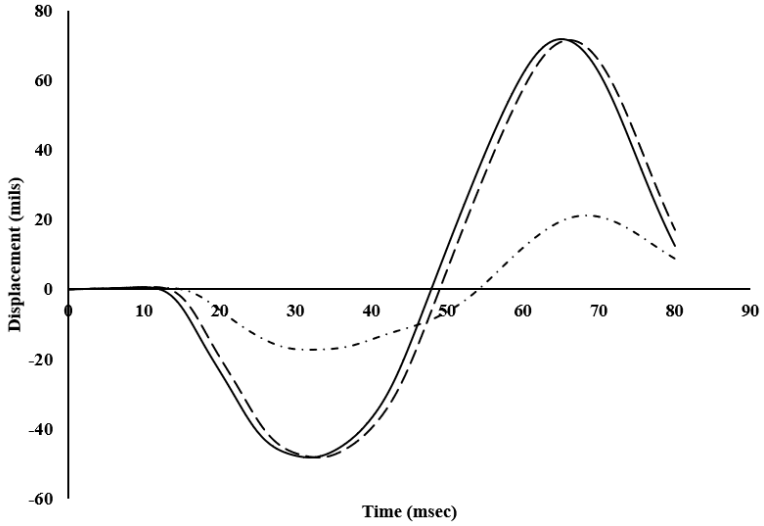

Figure 5. Corresponding displacements recorded in the same three calibration tests conducted by MDT in December 2019.

The next important parameter that is required for three-dimensional dynamic modeling of FWD tests is the mechanical damping of the material. Any natural dynamic system has some degree of damping which is due to the energy loss caused by the internal friction in the intact material. Additionally, in nonintact material, damping could also occur due to the slippage along interfaces. In numerical modeling of systems, the magnitude and form of these energy losses should be reproduced by damping [25]. The natural damping in soils and rocks is mainly independent of the frequency, i.e., damping is hysteretic [25–27]. The numerical formulation of the hysteretic damping is based on modulus reduction curves which imply a nonlinear stress/strain curve. Some examples of the Modulus reduction curves for clay, sand, and concrete are shown in Figure 6 [28–32].

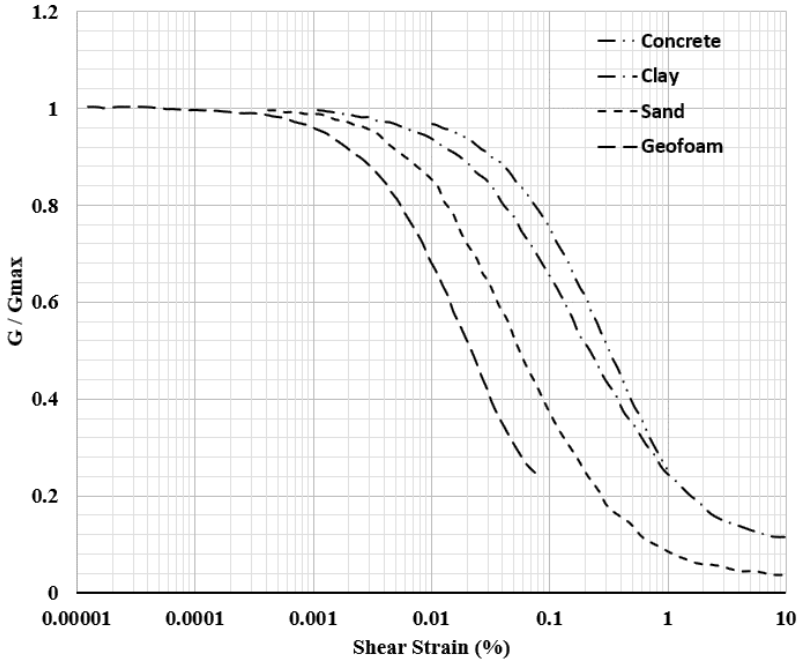

Figure 6. Some examples of the modulus reduction curves for clay, sand, and concrete (data from [28–32]).

Other important data required for modeling the calibration tests conducted by MDT have also been collected (from MDT or typical values) and summarized in Table 2.

Table 2. Summary of Material Properties Collected for Numerical Modeling

Material	Unit weight (pcf)	Elastic Modulus (psi)	Poisson's Ratio
Concrete	149.8	4.351E6	0.15
Sand Base and leveling Sand	120	3.472E3	0.1
Clay Subgrade	100	6.95E2	0.1
Geofoam (ESP19)	1.15	5.8E2	0.1

The next step in this project is to develop a model based on the original design (clay set up) and use the results of the previous calibration tests, i.e., deflection characteristics of the concrete slab, to validate the model. After validating the model developed in this step, the model will be adjusted to simulate the behavior of the preliminary alternative test area (geofoam set up). This model will also be validated using the results of calibration tests conducted on the geofoam setup. The final model will then be used to determine whether or not the use of geofoam instead of the clay layer is practically possible. If the results indicate that the replacement is possible, the model will be utilized to modify the preliminary alternative test area design to achieve deflection amplitudes that are in the acceptable range suggested by AASHTO R32-11.

7. NUMERICAL MODELING-ORIGINAL SETUP (TASK 2)

In this stage, a three-dimensional explicit finite volume model was developed based on the original design (i.e., clay set up as shown in Figure 1). As mentioned before, the deflection requirements by AASHTO R32 were met during the calibration tests conducted by MDT using this setup. FLAC3D (Fast Lagrangian Analysis of Continua in 3 Dimensions) software from Itasca Consulting Group, Inc. was used to create the model. The FISH script (code) developed in FLAC3D for this stage of modeling (task2) is presented in Appendix A.

7.1 Model Geometry and Initial Conditions

Four 12 ft wide (in X-direction) and 15 ft long (in Y-direction) blocks with different thicknesses (in Z-direction) were created for modeling the original test pit. Based on the original design, the thicknesses of the concrete slab, base sand, clay subgrade, and the leveling sand in the model were assigned as 5 in., 6 in., 48 in., and 1 in., respectively. The geometry of the test pit in the model is shown in Figure 7.

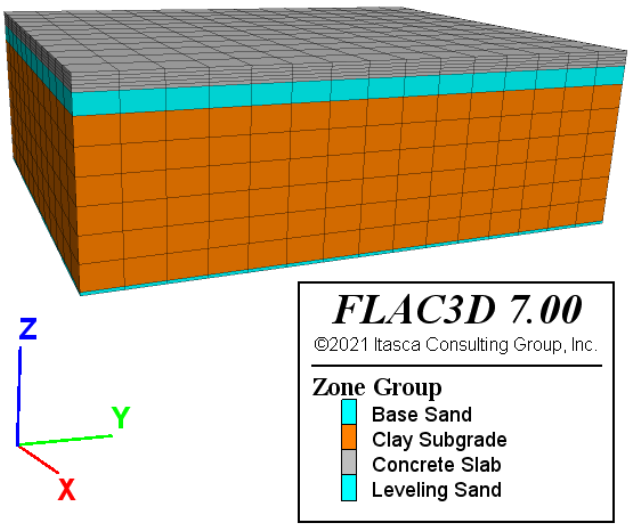

Figure 7. The geometry of the test pit model (original design) in FLAC3D.

The initial stress conditions, i.e., stress at any depth caused by the weight of overburden, were developed in the model and are shown in Figure 8.

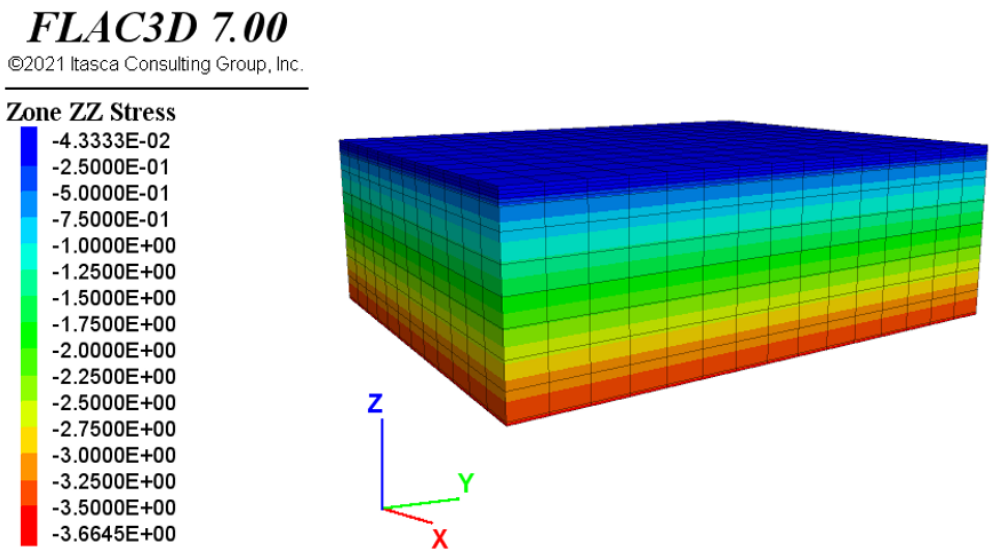

Figure 8. Initial Stress Conditions of the Model.

7.2 Boundary Conditions

In numerical modeling of the dynamic behavior of material, wave reflection at model boundaries could adversely affect the results of the model. This negative impact can be reduced by using free-field boundary conditions (also known as quiet or viscous boundaries) instead of fixed boundary conditions. Using these quiet boundaries in the modeling of the FWD tests on pavements (in the field) usually improves the predicted deflections by the model (e.g., [16,18]). In FWD calibration tests, however, the boundaries of the test pit are not completely under free-field conditions. In other words, there are actual physical boundaries around the test pit which means that the test pit is not continuously connected to the surrounding ground. This is especially the case for the clay subgrade where a liner is placed between the subgrade and the surrounding ground. To understand the effects of this discontinuity, both fixed and quiet boundary conditions were used in the model and the results were compared. In the model, we used free boundary conditions at the surface (top) of the model and fixed boundary conditions at the base (bottom), as well as all other four faces of the model, i.e., North, East, South, and West faces. We also tried quiet boundaries at the base and the other four faces of the model (except the surface). As was expected, due to the actual physical boundaries around the test pit, the fixed boundary conditions better simulated the calibration test pit behavior.

7.3 Material Constitutive Models and Material Properties

As mentioned before, different load magnitudes used in FWD calibration tests are within the elastic limits of all layers and linear elastic behavior has been commonly used in dynamic modeling of FWD tests [16,17,24]. Non-linear viscoelastic-plastic models and non-linear elastic material models with a Mohr-Coulomb yield have also been used for dynamic modeling of FWD tests ([4,18,33]). In this study, we tried both a linear elastic behavior with structural damping (hysteretic damping) and an elastoplastic material behavior with a Mohr-Coulomb yield model. Material properties used in both models are summarized in Table 3. The linear elastic model

with structural damping (hysteretic damping) simulated the behavior of the test pit more precisely.

Table 3. Material properties used in the model

Material	Unit weight (pcf)	Elastic Modulus (psi)	Poisson's Ratio	Cohesion (psi)	Friction Angle (degrees)
Concrete	149.8	4.351E6	0.15	337	46
Sand Base and leveling Sand	120	3.472E3	0.1	0	35
Clay Subgrade	100	6.95E2	0.1	7	29

As mentioned before, material damping was also considered in our models. Hysteretic damping was used based on the modulus reduction curves shown in Figure 6. Based on the modulus reduction curves, the following incremental constitutive relation for the shear strain can be derived [34]:

$$\bar{\tau} = M_s \gamma \tag{1}$$

$$M_t = \frac{d\bar{\tau}}{d\gamma} = M_s + \frac{dM_s}{d\gamma} \tag{2}$$

where, $\bar{\tau}$ is normalized shear stress, γ is the shear strain, M_s is the normalized secant modulus, and M_t is the normalized tangent modulus. The incremental shear modulus at any strain, G_γ, in the model is then calculated by:

$$G_\gamma = G_{max} M_t \tag{3}$$

$$G_{max} = \frac{E}{2(1+v)} \tag{4}$$

where, G_{max} is the maximum shear modulus (at zero strain), E is Young's modulus, and v is Poisson's ratio. In FLAC3D, different formulas can be used to fit the best curve to the actual modulus reduction curves from which the M_t (or M_s) at any strain is calculated during the modeling steps. The constants of the fitting formula are then given as inputs in FLAC3D. The following fitting formula, known as the sigma-3 fitting formula [34], was used in our model.

$$M_s = \frac{a}{1 + \exp(-\frac{L - x_0}{b})} \tag{5}$$

In Equation 5, L is the $\log_{10}(\gamma)$, and a, b, and x_0 are fitting constants. Table 4 summarizes the fitting constants for different layers used in our model.

Table 4. Fitting constant used for material damping in the model

Material	Constant a	Constant b	Constant x_0
Concrete	1.05	-0.5	-1.15
Sand Base and leveling Sand	1.07	-0.6	-0.63
Clay Subgrade	1.07	-0.55	-0.4

7.4 Impact Loads and Corresponding Displacements

As discussed before, the impact load time history data and corresponding displacements recorded during the calibration tests conducted on the clay test pit in 2016 are not available. The typical impact load time history shown in Figure 3 was therefore used in the model. The displacements (deflections) at the location of the sensors rack were then recorded at every step. For simplicity, a square area was used instead of a circular area to apply the impact loads in the model. Figure 9 shows the location of applied impact loads and the displacement sensors rack.

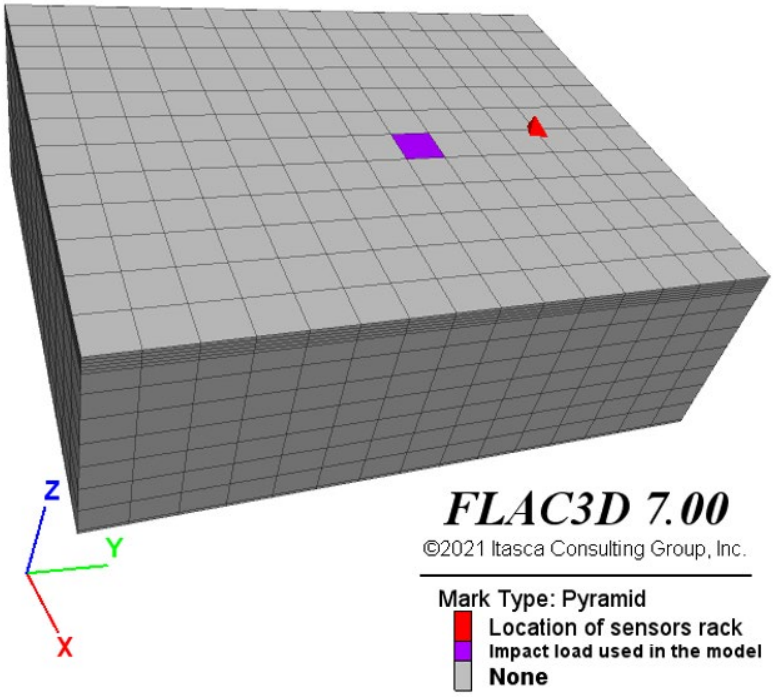

Figure 9. location of applied impact loads and the displacement sensors rack.

7.5 Results and Discussion

As explained before, the linear elastic models better simulated the behavior of the test pit. Therefore, only the results of linear elastic models with fixed boundary conditions are presented here. The displacement histories at the location of the sensors rack for all different impact loads are shown in Figure 10. The figure shows that the model's deflection history is consistent with the typical deflection patterns seen in the FWD calibration tests. The stress distribution and vertical displacement in the model 8 milliseconds after the weight drop are shown in Figure 11 and Figure 12, respectively.

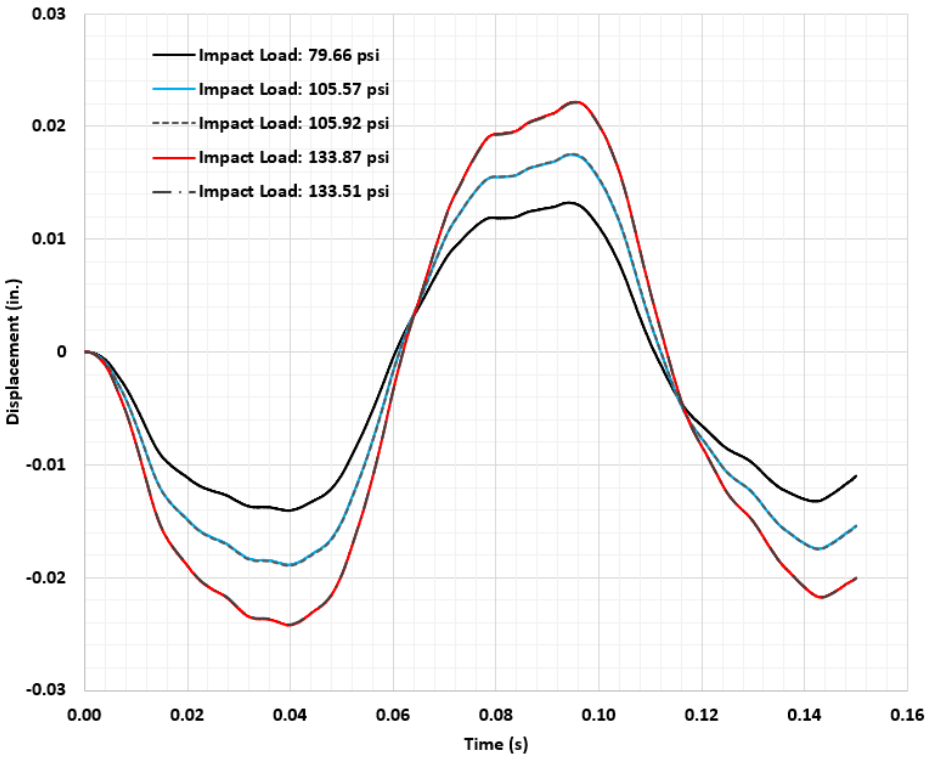

Figure 10. Displacement histories at the location of the sensors rack for five different impact loads.

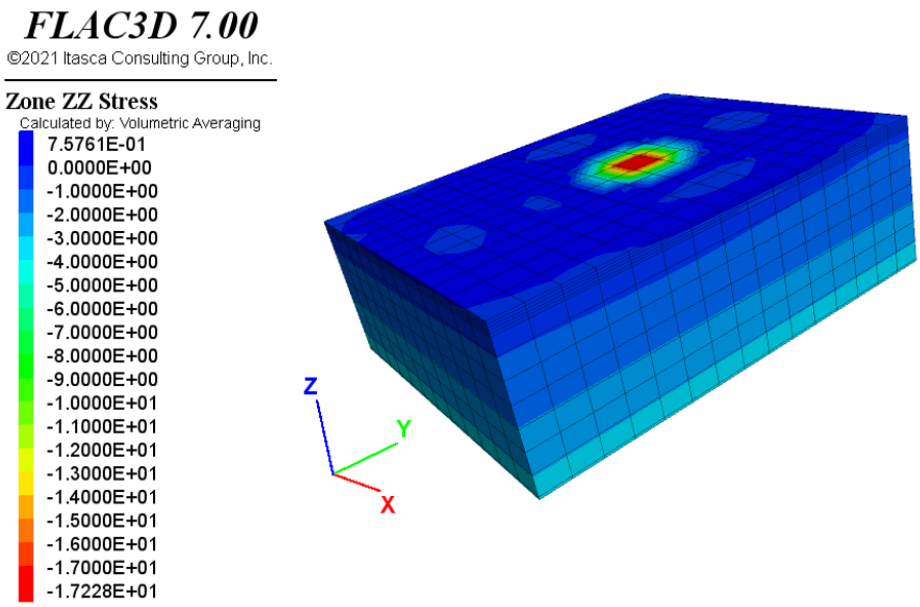

Figure 11. Stress distribution in the model (in psi), 8 miliseconds after the weight drop (for max impact load of 11.94 kips).

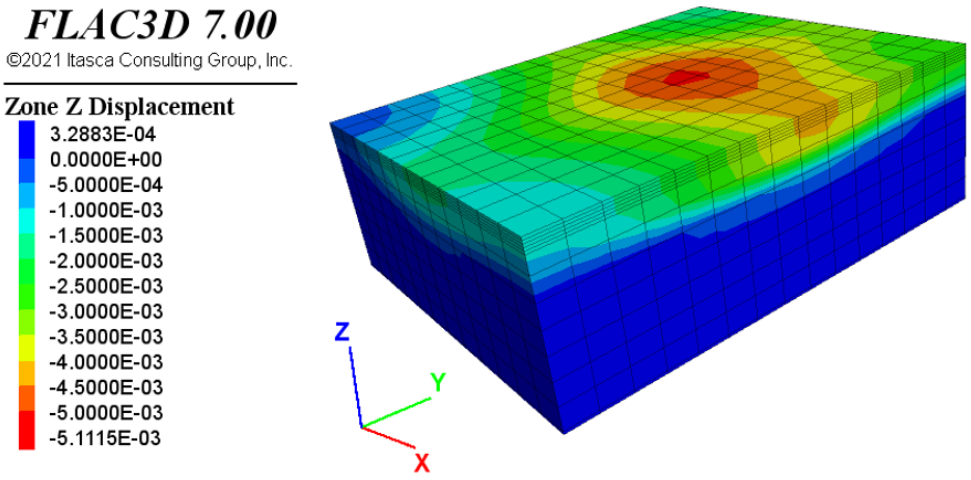

Figure 12. Vertical displacement of the model (in.), 8 milliseconds after the weight drop (for max impact load of 11.94 kips).

The maximum deflections predicted by the model for different load magnitudes, along with the recorded maximum deflections during the calibration tests are shown in Table 5.

Table 5. Summary of recorded and predicted deflections

Force (kips)	Maximum Stress (psi)	Recorded deflection (in)	Predicted deflection in the model (in)	Difference between recorded and predicted deflections (in)	Error (%)
9.01	79.665891	0.01413125	0.01406478	-0.00006647	-0.47
11.94	105.572779	0.01898625	0.01887952	-0.00010673	-0.56
11.98	105.926457	0.0190525	0.01894595	-0.00010655	-0.56
15.1	133.513314	0.0240775	0.02416509	0.00008759	0.36
15.14	133.866991	0.024075	0.02423262	0.00015762	0.65

As can be seen from the table, all the predicted deflections by the model are within 1% of recorded deflections during MDT's FWD tests. It is worth mentioning that the deflections predicted by the model are sensitive to the impact load time history used in the model. Although the impact load time histories are very consistent, a slight change in the form or the location of the peak of the history could change the predicted deflection histories. The model is also sensitive to the material properties as well as the location of the weight drop with respect to the location of the rack of sensors. The next step of this project is to modify the model developed in this step to simulate the behavior of the alternative calibration test pit (geofoam test pit). The main difference between the original clay set up (modeled in this step) and the alternative geofoam set up is that the clay subgrade is replaced with a geofoam subgrade that has significantly different elastic modulus and unit weight. Therefore, we are interested in understanding the sensitivity of the current model to the elastic modulus of the subgrade.

To achieve this goal, the model with the maximum impact load of 133.51 (psi) was rerun multiple times, each time with a different elastic modulus for the clay subgrade. All the other properties of the model were kept the same for this sensitivity analysis. The results of this sensitivity analysis are shown in Figure 13.

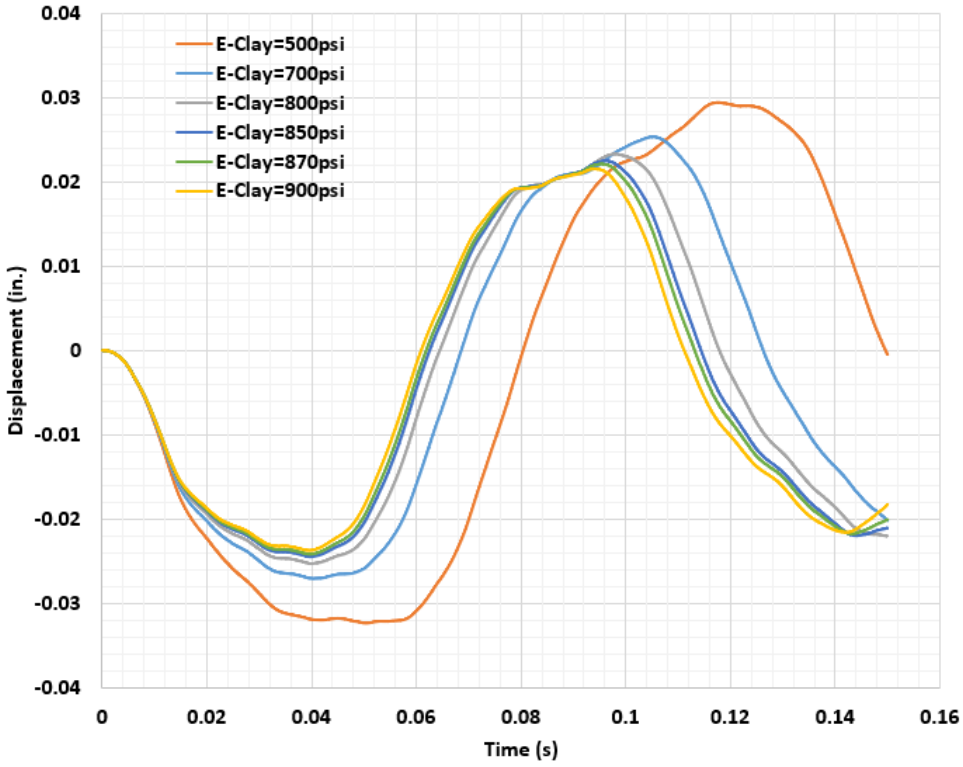

Figure 13. Sensitivity of the models predicted deflection histories to the Elastic Modulus of the Clay subgrade

As can be seen from Figure 13, reducing the elastic modulus of the subgrade increases the deflections of the model. This partly explains the excessive deflections observed in the MDT's geofoam test pit because the elastic modulus of geofoam is less than clay. The geometry of the MDT's alternative geofoam test pit is also slightly different from the original clay test pit, and the more precise analysis of its behavior will be investigated in the next step of this project.

7.6 Conclusions

The results of the second phase of this project (task 2) were to show the capability of the developed model in predicting the deflections with reasonable accuracy. The sensitivity of the model to the elastic modulus of the subgrade layer shows that the model is very likely capable of simulating the behavior of the alternative geofoam test pit. The behavior of the model can be assessed even better in the next step when both the impact load time history and measured deflection time history at the location of the sensors are known. This allows us to compare the predicted deflection time histories with the measured time histories instead of just comparing the maximum predicted and observed deflections.

8. REFERENCES

[1] AASHTO-R32-11. Calibrating the Load Cell and Deflection Sensors for a Falling Weight Deflectometer 2011.

[2] Irwin LH, Orr DP, Atkins D. FHWA-HRT-07-040, FWD Calibration Center and Operational Improvements: Redevelopment of the Calibration Protocol and Equipment. 2011.

[3] Irwin L, Yang W, Stubstad R. Deflection Reading Accuracy and Layer Thickness Accuracy in Backcalculation of Pavement Layer Moduli. Nondestruct. Test. Pavements Backcalc. Modul., ASTM International; 2008, p. 229-229–16. https://doi.org/10.1520/stp19810s.

[4] Kuo CM, Chou FJ. Development of 3-D finite element model for flexible pavements. J Chinese Inst Eng Trans Chinese Inst Eng A/Chung-Kuo K Ch'eng Hsuch K'an 2004;27:707–17. https://doi.org/10.1080/02533839.2004.9670918.

[5] Lytton R. Backcalculation of Pavement Layer Properties. Nondestruct. Test. Pavements Backcalc. Modul., ASTM International; 2008, p. 7-7–32. https://doi.org/10.1520/stp19797s.

[6] Chatti K, Kim TK. Simple dynamic backcalculation procedure for falling weight deflectometer testing of rigid pavements. Transp. Res. Rec., 2001, p. 30–8. https://doi.org/10.3141/1764-04.

[7] Khazanovich L, Booshehrian A. Dynamic viscoelastic analysis of falling weight deflectometer deflections for rigid and flexible pavements. Transp Res Rec 2015;2525:31–9. https://doi.org/10.3141/2525-04.

[8] Chatti K, Kim TK. Simple dynamic backcalculation procedure for falling weight deflectometer testing of rigid pavements. Transp. Res. Rec., National Research Council; 2001, p. 30–8. https://doi.org/10.3141/1764-04.

[9] Donovan P, Tutumluer E. Falling weight deflectometer testing to determine relative damage in asphalt pavement unbound aggregate layers. Transp Res Rec 2009:12–23. https://doi.org/10.3141/2104-02.

[10] Balzarini D, Chatti K, Zaabar I, Butt AA, Harvey JT. Mechanistic-Based Parametric Model for Predicting Rolling Resistance of Concrete Pavements. Transp Res Rec 2019;2673:341–50. https://doi.org/10.1177/0361198119847611.

[11] Meier RW, Rix GJ. Backcalculation of flexible pavement moduli using artificial neural networks. Transp Res Rec 1994:75–82.

[12] Meier R, Rix G. Backcalculation of flexible pavement moduli from dynamic deflection basins using artificial neural networks. Transp Res Rec J Transp Res Board 1995;1473:72–81.

[13] Khazanovich L. Dynamic Analysis of FWD Test Results for Rigid Pavements. Nondestruct. Test. Pavements Backcalc. Modul. Third Vol., 100 Barr Harbor Drive, PO Box C700, West Conshohocken, PA 19428-2959: ASTM International; 1999, p. 398-398–15. https://doi.org/10.1520/STP14780S.

[14] Kuo CM, Lin CC, Huang CH, Lai YC. Issues in simulating falling weight deflectometer test on concrete pavements. KSCE J Civ Eng 2016;20:702–8. https://doi.org/10.1007/s12205-015-0299-y.

[15] Foinquinos R, Roesset JM, Stokoe KH. Response of pavement systems to dynamic loads imposed by nondestructive tests. Transp Res Rec 1995:57–67.

[16] Mallela J, George KP. Three-dimensional dynamic response model for rigid pavements. Transp Res Rec 1448, TRB, Natl Res Counc Washington, DC 1994:92–9.

[17] Shoukry SN, William GW, Martinelli DR. Assessment of the performance of rigid pavement back-calculation through finite element modeling. In: Chase SB, editor. Nondestruct. Eval. Bridg. Highw. III, vol. 3587, SPIE; 1999, p. 146–56. https://doi.org/10.1117/12.339920.

[18] William GW. Backcalculation of pavement layers moduli using 3D nonlinear explicit finite element analysis. West Virginia University, 1999.

[19] Park K-C, Chang Y-C. An Analytical Study of Flexible Pavement Design Using Resilient Modulus Model of Expanded Polystyrene (EPS). J Korean Geosynth Soc 2015;14:35–44.

https://doi.org/10.12814/jkgss.2015.14.2.035.

[20] Riveros GA, Sadrekarimi A. Liquefaction resistance of Fraser River sand improved by a microbially-induced cementation. Soil Dyn Earthq Eng 2020;131:106034. https://doi.org/10.1016/j.soildyn.2020.106034.

[21] Newmark NM. Effects of earthquakes on dams and embankments. Geotechnique 1965;15:139–60.

[22] DeJong JT, Fritzges MB, Nüsslein K. Microbially Induced Cementation to Control Sand Response to Undrained Shear. J Geotech Geoenvironmental Eng 2006;132:1381–92. https://doi.org/10.1061/(ASCE)1090-0241(2006)132:11(1381).

[23] Falagán C, Grail BM, Johnson DB. New approaches for extracting and recovering metals from mine tailings. Miner Eng 2017;106:71–8. https://doi.org/10.1016/j.mineng.2016.10.008.

[24] Loizos A, Scarpas A. Verification of falling weight deflectometer backanalysis using a dynamic finite elements simulation. Int J Pavement Eng 2005;6:115–23. https://doi.org/10.1080/10298430500141030.

[25] Itasca. Dynamic Analysis. FLAC3D Version 6 User's Guid., Itasca Consulting Group Inc., Minneapolis, Minnesota, 1 USA; 2012.

[26] Wegel RL, Walther H. Internal dissipation in solids for small cyclic strains. J Appl Phys 1935;6:141–57. https://doi.org/10.1063/1.1745306.

[27] Gemant A, Jackson W. XCIII. The measurement of internal friction in some solid dielectric materials. London, Edinburgh, Dublin Philos Mag J Sci 1937;23:960–83. https://doi.org/10.1080/14786443708561868.

[28] Tiwari B, Ajmera B, Villegas D. Dynamic Properties of Lightweight Cellular Concrete for Geotechnical Applications. J Mater Civ Eng 2018;30:04017271. https://doi.org/10.1061/(asce)mt.1943-5533.0002155.

[29] Kishida T. Comparison and Correction of Modulus Reduction Models for Clays and Silts. J Geotech Geoenvironmental Eng 2017;143:04016110. https://doi.org/10.1061/(asce)gt.1943-5606.0001627.

[30] Pallav K, Raghukanth STG, Singh KD. Estimation of Seismic Site Coefficient and Seismic Microzonation of Imphal City, India, Using the Probabilistic Approach. Acta Geophys 2015;63:1339–67. https://doi.org/10.1515/acgeo-2015-0045.

[31] EPRI-TR-102293. Electric Power Research Institute: Guidelines for determining design basis ground motions. 1993.

[32] Athanasopoulos GA, Pelekis PC, Xenaki VC. Dynamic properties of EPS geofoam: An experimental investigation. Geosynth Int 1999;6:171–94. https://doi.org/10.1680/gein.6.0149.

[33] Rydén N. Surface Wave Testing of Pavements. University of Kansas, 2004.

[34] Itasca I. FLAC3D. V5 user manual 2012.

9. APPENDIX A - FLAC3D SCRIPT

The code used for modeling the behavior of MDT's FWD calibration test pit is presented here.

```
project new
model config dynamic
model dynamic active off

fish define MatMechPrprtes
;;Units: Length:in,  Density:snail/in3,   Force:lb, Stress:psi, Gravity: 386.04 in/s2
densityConcrete=2.245e-4
densityBaseSand=1.8e-4
densityClay=1.5e-4
densityLevelingSand=1.8e-4

FrictionConcrete=46
FrictionBaseSand=35
FrictionClay=29
FrictionLevelingSand=35

CohesionConcrete=337
CohesionBaseSand=0
CohesionClay=7
CohesionLevelingSand=0

Poison=0.1
PoisonConcrete=0.15
PoisonBaseSand=0.4
PoisonClay=0.2
PoisonLevelingSand=0.4

YoungConcrete=3.5e6
YoungBaseSand=4900
YoungClay=870
YoungLevelingSand=4900

end
@MatMechPrprtes

fish automatic-create on
model title 'MDT-FWD Calibration site'
;;  Generating the geometry (dimensions in inches)
zone create brick point 0 0 0 0 point 1 144 0 0 point 2 0 180 0 point 3 0 0 1 size 12 15 1 group 'Leveling Sand';
zone create brick point 0 0 0 1 point 1 144 0 1 point 2 0 180 1 point 3 0 0 49 size 12 15 6 group 'Clay Subgrade';
zone create brick point 0 0 0 49 point 1 144 0 49 point 2 0 180 49 point 3 0 0 55 size 12 15 1 group 'Sand Base';
zone create brick point 0 0 0 55 point 1 144 0 55 point 2 0 180 55 point 3 0 0 60 size 12 15 5 group 'Concrete Slab';
zone attach by-face tolerance-absolute 0.05

zone cmodel assign elastic
zone property young = 1e40 poiss = 0.1
zone property density @densityConcrete range group 'Concrete Slab'
zone property density @densityBaseSand range group 'Sand Base'
zone property density @densityClay range group 'Clay Subgrade'
zone property density @densityLevelingSand range group 'Leveling Sand'

model gravity 0 0 -386.04
zone initialize-stresses

zone gridpoint fix velocity-x range position-x 0.0
zone gridpoint fix velocity-y range position-x 0.0
zone gridpoint fix velocity-x range position-x 144
zone gridpoint fix velocity-y range position-x 144
```

```
zone gridpoint fix velocity-x range position-y 0.0
zone gridpoint fix velocity-y range position-y 0.0
zone gridpoint fix velocity-x range position-y 180
zone gridpoint fix velocity-y range position-y 180
zone gridpoint fix velocity-x range position-z 0
zone gridpoint fix velocity-y range position-z 0
zone gridpoint fix velocity-z range position-z 0

model largestrain off

zone cmodel assign elastic
zone property density @densityConcrete range group 'Concrete Slab'
zone property density @densityBaseSand range group 'Sand Base'
zone property density @densityClay range group 'Clay Subgrade'
zone property density @densityLevelingSand range group 'Leveling Sand'
zone property young @YoungConcrete poiss @PoisonConcrete range group 'Concrete Slab'
zone property young @YoungBaseSand poiss @PoisonBaseSand range group 'Sand Base'
zone property young @YoungClay poiss @PoisonClay range group 'Clay Subgrade
zone property young @YoungLevelingSand poiss @PoisonLevelingSand range group 'Leveling Sand'

model save 'FWD-Clay-1-InitialCondition'

model config dynamic
model restore 'FWD-Clay-1-InitialCondition'

plot create  'Geometry initial'
plot item create zone
plot item create structure-shell
plot item create axes
plot view projection perspective magnification 1 ...
center (72,90,27.5) eye (220.13,-193.34,86.485) roll 356.772 ...
clip-front -1e+10 clip-back 1e+10

plot create  'Zones ZZ-Stress'
plot item create zone active on contour stress quantity zz ...
method average ramp rainbow reversed on
plot item create axes
plot view projection perspective magnification 1 ...
center (72,90,27.5) eye (220.13,-193.34,86.485) roll 356.772 ...
clip-front -1e+10 clip-back 1e+10

plot create  'Zones Z-Displacement'
plot item create zone active on contour displacement component z log off ...
method average ramp rainbow reversed on
plot item create axes
plot view projection perspective magnification 1 ...
center (72,90,27.5) eye (220.13,-193.34,86.485) roll 356.772 ...
clip-front -1e+10 clip-back 1e+10

table '5' import 'SHISTPSINORM'

plot create  'Input Stress History'
Plot item create chart-table active on ...
table '5' name "Stress History" ...
axis-x label "Time (Sec)" exponent  show on value 1 auto on ...
axis-y label "Stress (psi)" exponent  show on value 2 auto on

model largestrain off
model dynamic active on

model history name='time' dynamic time-total
zone history name='szzCenter' stress-zz position (78 104 60)
```

```
zone history name='DispCenter' displacement-z position (78 104 60)
zone history name='DispSensor' displacement-z position (72 144 60)

zone dynamic damping hysteretic sigmoidal-3 1.05        -0.5   -1.15 range group 'Sand Base'
zone dynamic damping hysteretic sigmoidal-3 1.05        -0.5   -1.15 range group 'Leveling Sand'
zone dynamic damping hysteretic sigmoidal-3 1.07        -0.6   -0.63 range group 'Clay Subgrade'
zone dynamic damping hysteretic sigmoidal-3 1.07        -0.55 -0.4 range group 'Concrete Slab'

zone face apply stress-zz -133.51 table '5' time dynamic range position-x 72 84 position-y 96 108 position-z 60

plot create  'Stress center History'
plot item create chart-history active on ...
history 'szzCenter' name "szzCenter ZZ Stress at (72,96,55)" style line reversed-x off reversed-y off ...
style-line width 2 style solid color 'cyan' ...
alias "" ...
vs step reversed off ...
begin 0 end 0 skip 0 ...
axis-x log off minimum auto maximum auto inside on ...
label "Step" exponent  show on value 4 auto on ...
axis-y log off minimum auto maximum auto inside on ...
label "Y-Axis" exponent  show on value -1 auto on

plot create  'Displacement center History'
plot item create chart-history active on ...
history 'DispCenter' name "DispCenter Z Displacement at (72,90,55)" style line reversed-x off reversed-y off ...
style-line width 2 style solid color 'cyan' ...
alias "" ...
vs step reversed off ...
begin 0 end 0 skip 0 ...
axis-x log off minimum auto maximum auto inside on ...
label "Step" exponent  show on value 4 auto on ...
axis-y log off minimum auto maximum auto inside on ...
label "Y-Axis" exponent  show on value -37 auto on

plot create  'Displacement Sensor vs Step'
plot item create chart-history active on ...
history 'DispSensor' name "Displacement Sensor vs Step" style line reversed-x off reversed-y off ...
style-line width 2 style solid color 'cyan' ...
alias "" ...
vs step reversed off ...
begin 0 end 0 skip 0 ...
axis-x log off minimum auto maximum auto inside on ...
label "Step" exponent  show on value 4 auto on ...
axis-y log off minimum auto maximum auto inside on ...
label "Y-Axis" exponent  show on value -37 auto on

model solve dynamic time-total 0.008
model save 'FWD-Clay-2-8msecDynamic'

model solve dynamic time-total 0.010
model save 'FWD-Clay-2-10msecDynamic'

model solve dynamic time-total 0.012
model save 'FWD-Clay-2-12msecDynamic'

model solve dynamic time-total 0.018
model save 'FWD-Clay-2-18msecDynamic'

model solve dynamic time-total 0.020
model save 'FWD-Clay-2-20msecDynamic'

model solve dynamic time-total 0.022
```

```
model save 'FWD-Clay-2-22msecDynamic'

model solve dynamic time-total 0.025
model save 'FWD-Clay-2-25msecDynamic'

model solve dynamic time-total 0.030
model save 'FWD-Clay-2-30msecDynamic'

model solve dynamic time-total 0.060
model save 'FWD-Clay-2-60msecDynamic'

model solve dynamic time-total 0.15

history export 'szzCenter' vs 'time' table 'szzCenter.VS.DynamicTime'

plot create  'Stress center vs Dynamic time'
plot item create chart-table active on ...
table 'szzCenter.VS.DynamicTime' name "szzCenter.VS.DynamicTime" style line reversed-x off reversed-y off ...
style-line width 2 style solid color 'cyan' ...
alias "" ...
axis-x log off minimum auto maximum auto inside on ...
label "Dynamic Time (Seconds)" exponent  show on value -2 auto on ...
axis-y log off minimum auto maximum auto inside on ...
label "ZZ-Stress at center (psi)" exponent  show on value 0 auto on

history export 'DispCenter' vs 'time' table 'DispCenter.VS.DynamicTime'

plot create  'Stress center vs Dynamic time'
plot item create chart-table active on ...
table 'DispCenter.VS.DynamicTime' name "DispCenter.VS.DynamicTime" style line reversed-x off reversed-y off ...
style-line width 2 style solid color 'cyan' ...
alias "" ...
axis-x log off minimum auto maximum auto inside on ...
label "Dynamic Time (Seconds)" exponent  show on value -2 auto on ...
axis-y log off minimum auto maximum auto inside on ...
label "Center ZZ-Stress at center (psi)" exponent  show on value 0 auto on

history export 'DispSensor' vs 'time' table 'DispSensor.VS.DynamicTime'

plot create  'Sensor Displacement History'
plot item create chart-table active on ...
table 'DispSensor.VS.DynamicTime' name "Displacement at  Z Displacement at Sensor location" style line reversed-x
    off reversed-y off ...
style-line width 2 style solid color 'cyan' ...
alias "" ...
axis-x log off minimum auto maximum auto inside on ...
label "Dynamic Time (Seconds)" exponent  show on value 4 auto on ...
axis-y log off minimum auto maximum auto inside on ...
label "Z Displacement at Sensor location" exponent  show on value -37 auto on


zone face list apply conditions

table list
zone list stress range  position-x 72 84 position-y 98 110 position-z 60

model save 'FWD-Clay-2-0.15secDynamic-end'

table 'DispSensor.VS.DynamicTime' export 'Deflection' csv
```